Inductive Power Transfer Converter With Center-Tapped Pickup Winding

Yao-Ching Hsieh, *Member, IEEE*, Chia-Wei Chu, Hong-Wei Chang, and Cheng-Yi Lin

***Abstract*—A step-down wireless power transfer converter with center-tapped pickup windings is proposed in this article. The pickup winding is split into two sections and only one is connected to the load. This topology is more suitable for low-voltage level applications, such as consumer electronic products. Like the conventional series–parallel compensation technique, the circuit does not induce high circulation current at the transmitter coil under light load operation. The loosely coupled coils are analyzed with mutual inductance model; in addition, the input impedance and voltage gain are derived. The input impedance is proportional to the load impedance, and the voltage gain is less sensitive to the load variation. The proposed topology performs better than the conventional one at higher load conditions, especially when the coupling is poor. The efficiency of a laboratory circuit reaches 88.8% at best condition and it is higher than 63% ranging from 10- to 100-W load at 10- or 60-mm coil separation.**

***Index Terms*—Center-tapped, inductive power transfer, series-parallel compensation.**

I. Introduction

NEAR-FIELD electromagnetic induction techniques are widely applied on wireless power transfer (WPT) techniques nowadays. The applications range from small power requirements, such as the energizing of implanted medical devices [1], [2] to high-power traction motor drives [3]. Although there are two common methods for WPT, i.e., magnetic induction (or inductive power transfer, IPT) and electrostatic induction (or capacitive power transfer), IPT is more suitable for diversified power-level applications and longer induction distance [4], [5]. WPT techniques are able to improve mechanical reliability due to the freedom from plugging and unplugging. On-road wireless charging is also possible to reduce the on-board battery capacity requirement [3], [6]. However, the loose magnetic coupling produces higher self-inductance on both transmitter and pickup coils and also lower mutual inductance between them, which seriously impairs the transfer efficiency. Consequently, suitable compensation measures are required to reduce the impact of high self-inductance on both sides. For voltage-fed inverter circuit on the transmitter side, it is natural to adopt a series-connected capacitor to compensate the inductance effect [7]–[9]; nevertheless, there are some papers that propose current-fed topologies for driving the transmitter coils [10], [11]. Basically, the target of compensation is to enhance the power efficiency. For this purpose, the reactive power flowing in the circuit should be minimized; i.e., the phase angle of input impedance has to be zero [12], [13]. Besides, some other goals might also be pondered, such as locating the circuit operation at a load-independent constant voltage gain point [8], [14]. To pursue higher transfer efficiency, the coil design is also an important consideration. Higher quality factor is necessary to reduce the power loss on the coil itself, whereas higher mutual inductance is beneficial for maximizing the induction coupling. These two factors are highly influenced by coil separation and misalignment. To alleviate the influence from the mentioned factors, a polarized coupler topology, which is called *DD* coil, is presented in [15]. The flux coming from one *D*-shaped coil returns to another same-shaped coil on one side, whereas ferrite can be utilized to perfectly conduct the flux on the other side, meanwhile shielding the leakage flux. The work in [16] enhances the idea and extends into a quad *D* quadrature coil layout, or *QDQ*, to maintain high coupling coefficient and efficient power transfer during reasonable misalignment. In [17], pickup coil composed of horizontal and vertical coils, so-called quadrature coil, is proposed to enlarge the flux coupling. Usually, the current flowing through the winding turns within the coil is in a perfectly identical phase; however, as the current frequency increases to several megahertz, the phase difference would be more apparent or even opposite. This phenomenon is discussed in [18] and an alternative winding coil is proposed to alleviate this effect.

In [8], both series and parallel compensation on the pickup side are compared. It is concluded that although series compensation is possible to achieve maximized efficiency, it is load sensitive. On the other hand, parallel compensation is more suitable for load-variant applications. However, the voltage gain of a parallel-compensated IPT converter at the load-invariant frequency is much higher than that of a series-compensated one. Higher order resonant tanks are also employed to compensate the transmission. A transmitter-side *LCL* compensation is also proposed to reduce conduction loss on the circuit [19]. If the impedances of all three resonant components, i.e., two inductances and one capacitor, are matched, the inverter sees a pure resistive load while operating at the resonant frequency. A double-sided *LCC* compensation is proposed in [20]. Nearly unity power

Manuscript received November 23, 2020; revised February 5, 2021 and April 6, 2021; accepted May 15, 2021. Date of publication May 18, 2021; date of current version July 30, 2021. This work was supported by the Ministry of Science and Technology, Taiwan, under Projects MOST 107-2221-E-110-017 and MOST 109-2221-E-110-026. Recommended for publication by Associate Editor J.-I. Itoh. *(Corresponding author: Yao-Ching Hsieh.)*

The authors are with the Electrical Engineering Department, National Sun Yat-sen University, Kaohsiung 80424, Taiwan (e-mail: ychsieh@mail.ee.nsysu.edu.tw; oweiiii0011@gmail.com; m073010043@g-mail.nsysu.edu.tw; a0910504263@gmail.com).

Color versions of one or more figures in this article are available at https://doi.org/10.1109/TPEL.2021.3081598.

Digital Object Identifier 10.1109/TPEL.2021.3081598

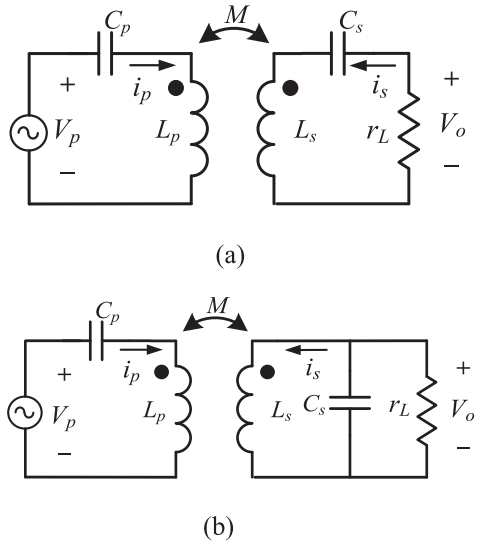

Fig. 1. Capacitor compensation networks. (a) Series–series compensation. (b) Series–parallel compensation.

factor can be achieved with no dependence on coupling and load conditions. Thus, a high-efficiency WPT system can be achieved. Load-independent output is another concern. Research works in [21] and [22] proposed switch-controlled capacitors to match the resonant frequency, while the research work in [23] integrated different topologies to realize the misalignment.

This article proposes a novel pickup winding composed of two identical subwindings, i.e., center-tapped pickup winding. One of the subwindings is connected with a rectifier and then to the load. By this modification, the voltage gain can be reduced and more suitable for low-voltage applications, such as consumer electronics and battery charging. By the proposed topology and compensation capacitor selections, the circuit performs more efficiently compared with conventional compensation methods, especially when the coils are more separated. The following of this article is organized as follows. Section II discusses the compensations. Section III introduces the proposed center-tapped pickup winding. Section IV illustrates the operation mode analysis of the proposed converter. Section V provides the experimental results for verification. Finally, Section VI concludes the article.

II. Discussions on Resonant Compensation

Since there is no strong coupling between transmitter and pickup windings for IPT systems, high self-inductances and low mutual coupling on both windings result in high-voltage drops and low-power transmission efficiency. Capacitors are usually applied to overcome the inductive voltage drops. As illustrated in Fig. 1, series–series (SS) and series–parallel (SP) compensations are commonly employed [7]. If the secondary network is reflected back to the primary side, the input impedance from the voltage source for SS and SP compensations are formulated as follows:

$$\begin{cases} Z_{\text{in,SS}} = j\omega L_p + \frac{1}{j\omega C_p} + \frac{\omega^2 M^2}{j\omega L_s + \frac{1}{j\omega C_s} + r_L} \\ Z_{\text{in,SP}} = j\omega L_p + \frac{1}{j\omega C_p} + \frac{\omega^2 M^2 (1 + j\omega C_s r_L)}{r_L + j\omega L_s - \omega^2 L_s C_s r_L}. \end{cases} \tag{1}$$

Conventionally, the system operation frequency is chosen so that the inductive and capacitive impedances cancel each other on both sides, i.e.,

$$\omega = \frac{1}{\sqrt{L_p C_p}} = \frac{1}{\sqrt{L_s C_s}}. \tag{2}$$

Therefore, (1) can be simplified as follows:

$$\begin{cases} Z_{\text{in,SS}} = \frac{\omega^2 M^2}{r_L} \\ Z_{\text{in,SP}} = \frac{r_L M^2}{L_s^2} - j\omega \frac{M^2}{L_s}. \end{cases} \tag{3}$$

Equation (3) shows that actually SP case does not reach resonance by this compensation method, i.e., the input reactance does not reduce to zero. This implies that the energy efficiency is not optimized by this compensation method. On the other hand, for the SS case, the impedance is inversely proportional to load resistance r_L; that is, under light load condition, $Z_{\text{in,SS}}$ becomes very small. This implies a large circulating current occurs on the primary winding for the SS case. Moreover, the current flowing through the transmitter and pickup windings as well as the voltage gains (V_o/V_p) for both cases can be formulated as follows:

$$\begin{cases} I_{p,\text{SS}} = \frac{r_L}{j\omega M} I_o \\ I_{p,\text{SP}} = \frac{L_s}{M} I_o \end{cases} \tag{4}$$

$$\begin{cases} I_{s,\text{SS}} = I_o \\ I_{s,\text{SP}} = -(1 + j\omega C_s r_L) I_o \end{cases} \tag{5}$$

$$\begin{cases} G_{\text{SS}} = \frac{\omega M}{r_o} \\ G_{\text{SP}} = \frac{r_L L_s}{M(r_L - j\omega L_s)}. \end{cases} \tag{6}$$

Equation (6) reveals that the voltage gain is apparently affected by load condition for SS, whereas for SP, the influence is partly canceled due to the presence of r_L simultaneously at numerator and denominator. To sum up, by the compensation option of (2), SP is more suitable for applications with wider load variation, such as battery charging. Contrarily, for heavy-load applications, the SS case is able to present higher efficiency.

III. Proposed Center-Tapped Pickup Winding

For most wireless charging applications, especially for consumer electronics, the voltage level is much lower than that of the utility source. Usually, the windings for IPT should be operated at a high voltage level to achieve higher efficiency. For SP compensation, its voltage gain is higher than unity; that is, a dc–dc converter with high-voltage step-down ratio is required to regulate the output voltage to a suitable level. Unfortunately, the higher step-down ratio requirement is possible to impair the overall efficiency of dc–dc converters. In this article, the pickup winding is split into two center-tapped subwindings, and the output is extracted out from one subwinding; therefore, the output voltage can be reduced without increasing the winding current. Fig. 2 illustrates the proposed IPT converter with center-tapped windings. To analyze the circuit, the nonideal features of active switches, diodes, and capacitors are neglected. An equivalent circuit in Fig. 3 is obtained by using fundamental harmonics analysis. The windings are modeled as mutual inductances,

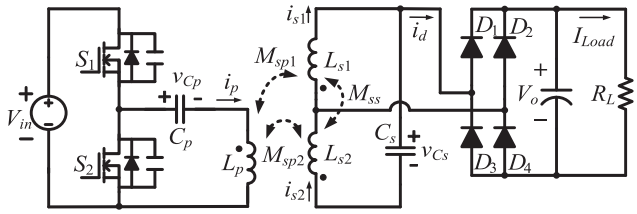

Fig. 2. Proposed center-tapped pickup winding inductive power transfer converter.

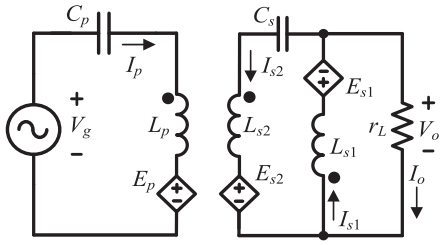

Fig. 3. Equivalent circuit with the proposed windings.

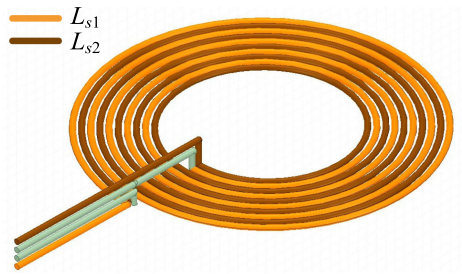

Fig. 4. Implementation illustration of center-tapped pickup winding.

whereas the dc source, i.e., $V_{\rm in}$, and load resistance, i.e., $R_{\rm L}$, are reflected to the ac side and replaced by $V_{\rm g}$ and r_L, respectively. Without loss of generality, the self-inductances, i.e., $L_{\rm s1}$ and $L_{\rm s2}$, are assumed to be equal; moreover, the mutual inductances between transmitter and pickup windings, i.e., $M_{\rm sp1}$ and $M_{\rm sp2}$, are also identical. That is, $L_{\rm s1} = L_{\rm s2} = L_{\rm sc}$ and $M_{\rm sp1} = M_{\rm sp2} = M_{\rm sp}$ are assumed.

Fig. 4 illustrates an example of how to implement the center-tapped pickup winding. Two multithread wires are parallel wound to form the two subwindings, and they are tail to head connected. This arrangement provides better coupling between two subwindings; on the other hand, the symmetrical coupling between pickup and transmitter windings can also be obtained.

The induced voltage on transmitter and the pickup windings, i.e., E_p, E_{s1}, and E_{s2}, can be expressed as follows:

$$\begin{cases} E_p = j\omega M_{\rm sp}\left(I_{s1} + I_{s2}\right) \\ E_{s1} = j\omega M_{\rm sp} I_p + j\omega M_{\rm ss} I_{s2} \\ E_{s2} = j\omega M_{\rm sp} I_p + j\omega M_{\rm ss} I_{s1}. \end{cases} \tag{7}$$

From KCL and KVL, the following equations can also be derived:

$$I_{s1} = I_{s2} + I_o \tag{8}$$

$$\begin{cases} E_{s1} = -I_o r_L - j\omega L_{s1} I_{s1} \\ E_{s2} = I_o r_L - j(\omega L_{s2} - \frac{1}{\omega C_s}) I_{s2}. \end{cases} \tag{9}$$

Organizing (7)–(9), the relation between transmitter winding current, i.e., I_p, and output current, i.e., I_o, can be formulated as follows:

$$\begin{aligned} j\omega M_{\rm sp} I_p = & \left[-r_L + 2r_L\omega^2(L_{\rm sc} + M_{\rm ss})C_s \right. \\ & \left. - j\omega(\omega^2 C_s {M_{\rm ss}}^2 - \omega^2 C_s {L_{\rm sc}}^2 + L_{\rm sc})\right] I_o. \end{aligned} \tag{10}$$

Define the resonant frequency of the pickup winding as ω_{r2}, and the compensation capacitor C_s is chosen such that

$$\omega = \omega_{r2} = \frac{1}{\sqrt{2(L_{\rm sc} + M_{\rm ss})C_s}}. \tag{11}$$

Therefore, (8) can be simplified as follows:

$$I_p = -\frac{L_{\rm sc} + M_{\rm ss}}{2M_{\rm sp}} I_o. \tag{12}$$

Also, by organizing (7)–(9), two pickup winding currents can be written as

$$\begin{cases} I_{s1} = \left[\frac{3M_{\rm ss}+L_{\rm sc}}{2(M_{\rm ss}+L_{\rm sc})} + j\frac{r_L}{\omega(M_{\rm ss}+L_{\rm sc})}\right] I_o \\ I_{s2} = \left[\frac{M_{\rm ss}-L_{\rm sc}}{2(M_{\rm ss}+L_{\rm sc})} + j\frac{r_L}{\omega(M_{\rm ss}+L_{\rm sc})}\right] I_o. \end{cases} \tag{13}$$

The above equation depicts that there is a circulation current flowing through the two pickup windings. Moreover, when the load resistance r_L is higher, i.e., at a lighter load, the circulation current is even larger. The relation between E_p and I_p can be derived as follows:

$$E_p = \left[\frac{4{M_{\rm sp}}^2 r_L}{(L_{\rm sc}+M_{\rm ss})^2} - j\omega\frac{4{M_{\rm sp}}^2 M_{\rm ss}}{(L_{\rm sc}+M_{\rm ss})^2}\right] I_p. \tag{14}$$

Accordingly, the voltage fed into the resonant circuit is

$$\begin{aligned} V_g = & \left[\frac{4{M_{\rm sp}}^2 r_L}{(L_{\rm sc}+M_{\rm ss})^2} - j\omega\frac{4{M_{\rm sp}}^2 M_{\rm ss}}{(L_{\rm sc}+M_{\rm ss})^2}\right. \\ & \left. + \left(j\omega L_P + \frac{1}{j\omega C_p}\right)\right] I_p. \end{aligned} \tag{15}$$

The real power and reactive power fed into the resonant tank are as follows:

$$\begin{cases} P_{\rm in} = {\rm Re}\left\{V_g {I_p}^*\right\} = \frac{4{M_{\rm sp}}^2 r_L}{(L_{\rm sc}+M_{\rm ss})^2} I_p^2 = I_o^2 r_L \\ Q_{\rm in} = {\rm Im}\left\{V_g {I_p}^*\right\} = \left[-\omega\frac{4{M_{\rm sp}}^2 M_{\rm ss}}{(L_{\rm sc}+M_{\rm ss})^2} + \left(\omega L_p - \frac{1}{\omega C_p}\right)\right] I_p^2. \end{cases} \tag{16}$$

To minimize the winding loss, the reactive power, i.e., $Q_{\rm in}$, is set to be zero. Let switching frequency ω be equal to ω_{r2}, the compensation capacitor, i.e., C_p, of transmitter side should be

$$C_p = \left\{{\omega_{r2}}^2\left[L_p - \frac{4M_{\rm ss}{M_{\rm sp}}^2}{(L_{\rm sc} + M_{\rm ss})^2}\right]\right\}^{-1}. \tag{17}$$

The input impedance can be expressed as follows:

$$Z_{\rm in} = \frac{V_g}{I_p} = \frac{4{M_{\rm sp}}^2 r_L}{(L_{\rm sc} + M_{\rm ss})^2}. \tag{18}$$

The voltage gain, i.e., G_v, of the resonant circuit can be obtained as follows:

$$G_v \equiv \frac{V_o}{V_g} = \frac{I_o r_L}{V_g} = \frac{L_{\rm sc} + M_{\rm ss}}{2M_{\rm sp}}. \tag{19}$$

Comparing the input impedance of (3) and (18), the proposed winding does not suffer from the inverse proportionality problem in SS compensation; it also gets rid of the reactance part as in SP compensation. As for voltage gain comparison of (6) and

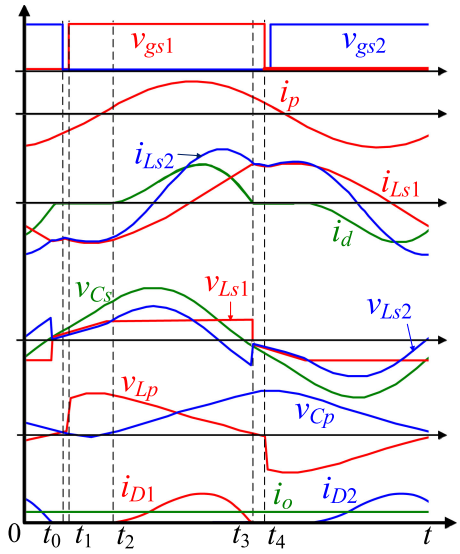

Fig. 5. Theoretical waveforms.

(19), unlike the SS and SP cases, the proposed solution is load independent.

IV. Circuit Operation

Fig. 5 illustrates the theoretical waveforms of the proposed IPT converter. There are eight intervals within one switching cycle. Due to similarity, only the first four intervals are discussed here, and Fig. 6 shows the current conduction path for each interval.

Interval I [$t_0 \le t < t_1$, see Fig. 6(a)]:

At t_0, switch S_2 turns OFF, transmitter winding current discharges and charges the output capacitances of S_1 and S_2 respectively. As the voltage across S_1 decreases to zero, it is ready for ZVS on S_1.

Interval II [$t_1 \le t < t_2$, see Fig. 6(b)]:

At t_1, the voltage across S_2 reaches to $V_{\rm in}$, whereas S_1 remains conducting. Current i_p turns from negative to positive, which makes $v_{\rm Cp}$ reaches its minimum value during this interval. The voltage fed into the transmitter resonant tank is a rectangular waveform with its fundamental component slightly phase leading to i_p. Both currents $i_{\rm Ls1}$ and $i_{\rm Ls2}$ are negative and of the same magnitude; that is, capacitor C_s is replenished and $v_{\rm Cs}$ increases. Due to the similarity between the center-tapped windings, $v_{\rm Ls1}$ approximately is half of $v_{\rm Cs}$, which is lower than the output voltage, $V_{\rm Co}$. Hence, the rectifier diodes are all reverse biased.

Interval III [$t_2 \le t < t_3$, see Fig. 6(c)]:

At t_2, $v_{\rm Ls1}$ is high enough to forward bias diodes D_1 and D_4, and $v_{\rm Ls1}$ is clamped at V_o afterward. However, L_{s2} continues resonating with C_s; therefore, $v_{\rm Cs}$ and $i_{\rm Ls2}$ remain in sinusoidal waveforms. Since $i_{\rm Ls1}$ and $i_{\rm Ls2}$ vary in distinct rate, their difference current, i.e., i_d, flows through the rectifier to the load.

Interval IV [$t_3 \le t < t_4$, see Fig. 6(d)]:

At t_3, resonating $i_{\rm Ls2}$ becomes equal to linearly varying $i_{\rm Ls1}$ again, which forces D_1 and D_4 to stop conducting. The identical positive $i_{\rm Ls1}$ and $i_{\rm Ls2}$ extracts charge out of C_s, making $v_{\rm Cs}$ vary toward negative. The load current I_o is supplied by C_o. Switch

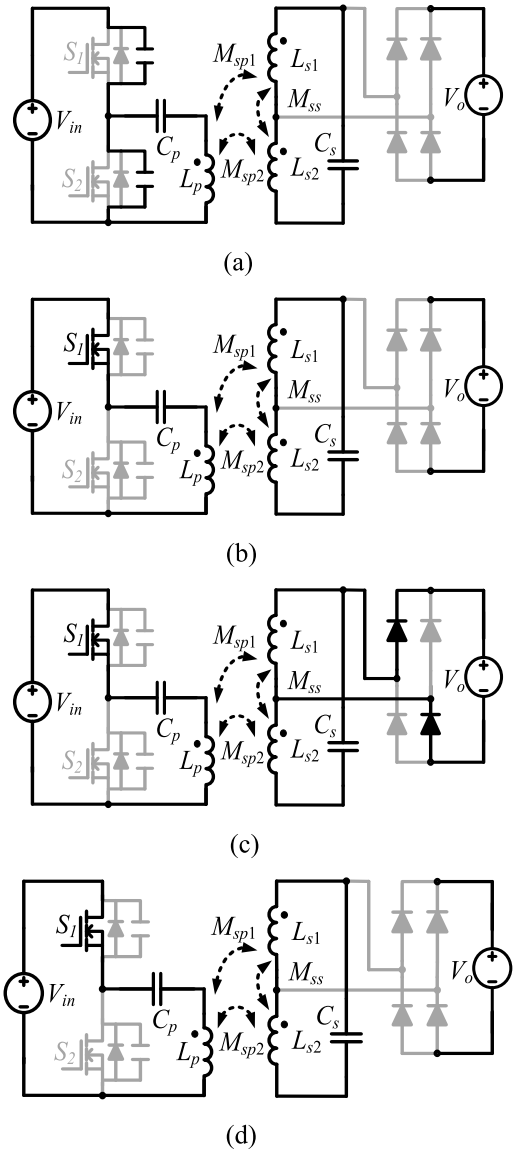

Fig. 6. Operation intervals. (a) Interval I. (b) Interval II. (c) Interval III. (d) Interval IV.

S_1 turns OFF at t_4, the operation is similar to that at t_0, which initiates the scenario of the negative half cycle.

V. Experimental Results

The windings are wound on a plane of 15-cm diameter and the distance between transmitter and pickup windings is 10 mm. Transmitter winding consists of 12 turns, whereas pickup winding is composed of two four-turn subwindings. To increase the magnetic field and enhance the coupling between transmitter and pickup windings, eight I-type AT2.1K high-frequency ferrite cores, with 60-mm length, 15-mm width, and 4-mm thickness, are radially deployed outside the windings. The conductors applied are 0.1-mm-diameter, 400 threads Litz wire to minimize skin effect. The circuit parameters are listed in Table I. The self- and mutual inductances are measured by an *LCR* meter, and the capacitance values are calculated from (11) and (17). The

TABLE I
CIRCUIT PARAMETERS

Operation frequency, f_s	140 kHz
Transmitter self-inductance, L_p	21.75 μH
Pickup self-inductance, L_{s1}/L_{s2}	3.91/3.85 μH
Mutual inductances, M_{sp1}/M_{sp2}	4.3/4.32 μH
Mutual inductance, M_{ss}	3.2 μH
Resonant capacitor, C_p/C_s	75/90 nF
Output capacitor, C_o	330 μF

TABLE II
SIMULATED INDUCTANCES WITH DIFFERENT CORE NUMBERS

parameters	4 cores	8 cores	12 cores
L_p	21.69 μH	26.76 μH	28.79 μH
L_{ss}	4.44 μH	5.47 μH	5.79 μH
M_{sp}	6.57 μH	8.71 μH	9.48 μH
M_{ss}	4.23 μH	5.27 μH	5.61 μH

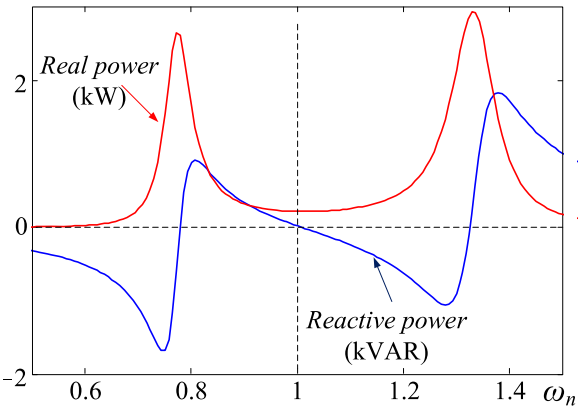

Fig. 7. Simulated input power.

capacitors are constructed with five and six pieces of 15 nF/1000 V off-the-shelf metalized film capacitors. The active switches are IRFB4332PbF MOSFETs, whereas the diodes are STPS30100ST. Table II shows the simulated results of deploying 4, 8, and 12 ferrite cores outside the windings. Surely, more ferrite cores will produce higher inductances, however, 12-core case only improves a little. Therefore, eight cores are adopted in this article. Equations (15) and (16) are applied to calculate the input complex power, and the input real power and reactive power can be graphically represented as in Fig. 7, where ω_n is defined as ω/ω_{r2} and the parameters are given in Table I. It can be seen that the reactive power is almost zero, whereas the real power is insensitive to frequency variation around the frequency of unity ω_n.

Fig. 8 is the photograph of the whole system. The ferrite cores are placed at the outer sides to confine the flux. High permeability and high resistivity soft magnetics is preferred for this purpose. Since the main purpose of the experiments

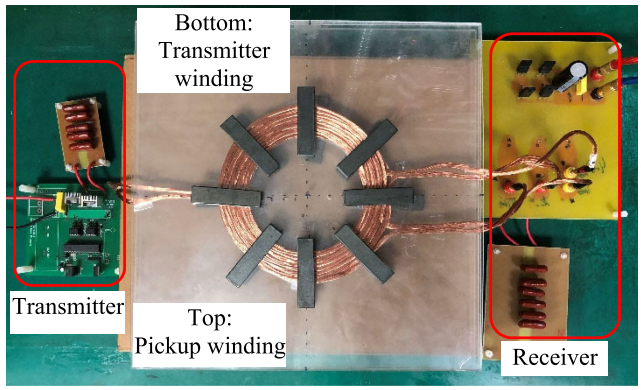

Fig. 8. Photograph of the proposed IPT system.

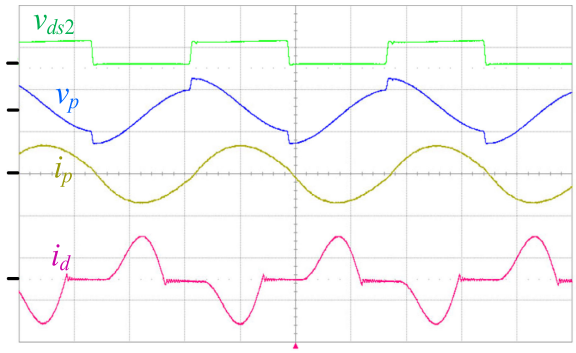

(i_p, i_d: 10 A/div; v_p: 200 V/div; v_{ds2}: 100 V/div; time: 2 μs/div)
(a)

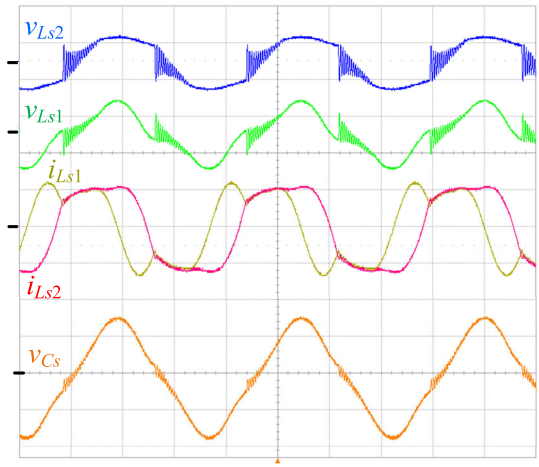

(i_{Ls1}, i_{Ls2}: 5 A/div; v_{Ls2}, v_{Ls1}, v_{Cs}: 50 V/div; time: 2 μs/div)
(b)

Fig. 9. Waveforms at 100-W load and 10-mm separation. (a) Transmitter side and diode current. (b) Pickup side.

is to verify the operation of the proposed topology, the voltage regulation is not considered. Furthermore, since the best compensation usually would happen within a small range or even only at one specific frequency, the frequency modulation for IPT converters is not preferred to meet the load adaption. Contrarily, a high-efficiency extra converter usually would be a better solution than to modulate operation frequency of the IPT

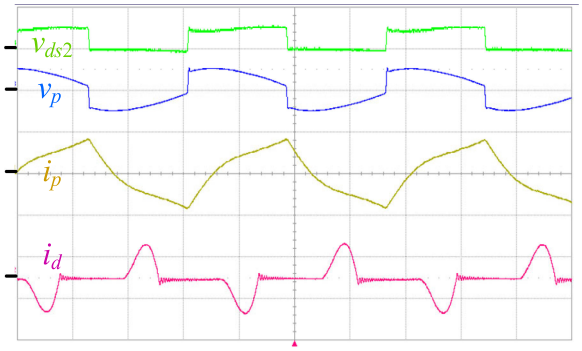

(i_p, i_d: 2 A/div; v_p, v_{ds2}: 100 V/div; time: 2 μs/div)
(a)

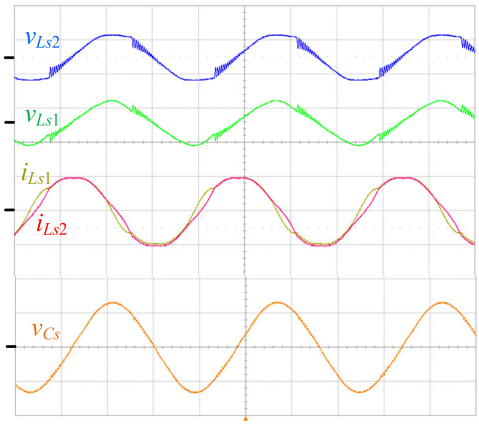

(i_{Ls1}, i_{Ls2}: 5 A/div; v_{Ls2}, v_{Ls1}, v_{Cs}: 50 V/div; time: 2 μs/div)
(b)

Fig. 10. Waveforms at 10-W load and 10-mm separation. (a) Transmitter side and diode current. (b) Pickup. side.

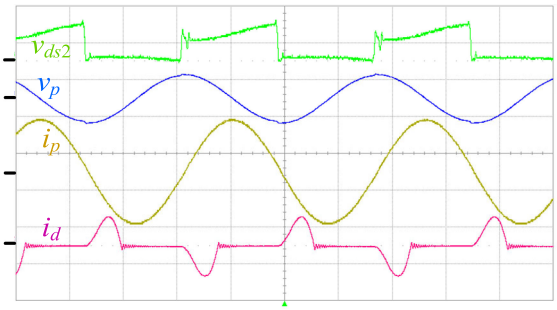

(i_p: 5 A/div; i_d: 2 A/div; v_p: 200 V/div; v_{ds2}: 10 V/div; time: 2 μs/div)
(a)

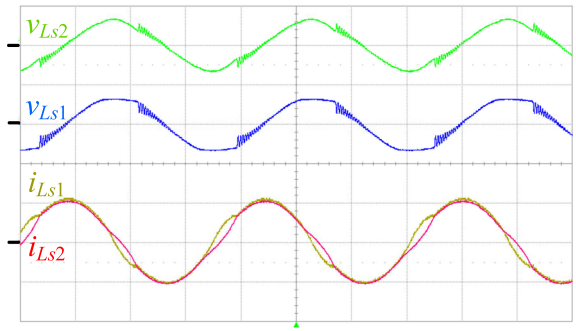

(i_{Ls1}, i_{Ls2}: 5 A/div; v_{Ls2}, v_{Ls1}, v_{Cs}: 50 V/div; time: 2 μs/div)
(b)

Fig. 11. Waveforms at 10-W load and 60-mm separation. (a) Transmitter side and diode current. (b) Pickup. side.

converter. Therefore, the following experiments are open-loop controlled and the input voltage is adjusted to obtain required output voltage and power.

Fig. 9 shows the experimental waveforms of the proposed IPT converter with 10-mm separation between transmitter and pickup windings at 100 W output power. Fig. 9(a) shows mainly the transmitter-side waveforms and Fig. 9(b) demonstrates the pickup-side waveforms. Current i_p slightly lags the fundamental component of voltage $v_{\rm ds2}$ as expected. The peak transmitter winding current and output diode current are about 6.3 and 9.2 A, respectively. As i_d becomes zero, the reverse recovery will cause the ringing at voltages $v_{\rm Ls1}$, $v_{\rm Ls2}$, and $v_{\rm Cs}$. As i_d is nonzero, the voltages across L_{s1} and L_{s2} are different as well as the current variation rates. The current difference forms the diode current i_d.

Fig. 10 shows the waveforms at light load of 10 W and similarly 10-mm separation. Due to the higher load impedance, the transmitter winding current and the difference between the pickup subwindings are both much smaller. However, the subwinding currents almost remain as large as those at heavy load, and so does the voltage $v_{\rm Cs}$, which means that the light load efficiency is lower due to the loss on pickup winding. Nevertheless, the similar problem emerges in conventional SP-compensated IPT converters. It is also noted that since total five channels are required to monitor the waveforms in Figs. 9(b) and 10(b), the $v_{\rm Cs}$ waveform is obtained separately. However, the same trigger level and time lag with $v_{\rm Ls2}$ are set for the two screenshots and then the waveforms are combined into one figure for convenience of inspection.

The coil separation is then increased to 60 mm. Fig. 11 shows the waveforms at 10 W output power. Compared with those in Fig. 10, the waveforms are similar on the pickup side; however, the transmitter side current and voltage are much higher. This is because that no matter how separated the coils, the pickup side voltage and current are directly related to the output. However, the longer separation causes a lower mutual inductance; therefore, higher current and voltage on the transmitter are required to produce enough output at the pickup side. As a result, the efficiency is lower.

Fig. 12 illustrates the waveforms of conventional SP WPT for comparison with Fig. 11. The separation and output power are identical with 60 mm and 10 W. For the pickup side, part of the coil current, i.e., i_s, forms the diode current i_d, whereas the diode current is the difference of $i_{\rm Ls1}$ and $i_{\rm Ls2}$ for the center-tapped pickup case. For the transmitter side, the waveforms are very similar except the coil current is higher for the proposed circuit. Therefore, the proposed circuit has lower efficiency at worse coupling and light load conditions.

Fig. 13 depicts the power efficiency comparison on the conventional SP IPT and the proposed center-tapped circuit. The

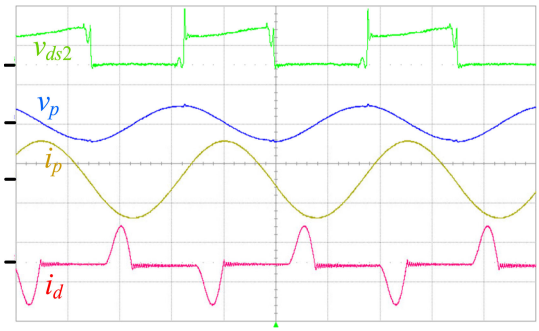

(i_p: 5A/div; i_d: 2A/div; v_p: 200V/div; v_{ds2}: 10V/div; time: 2μs/div)
(a)

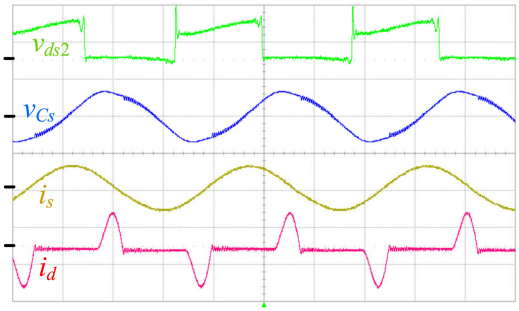

(i_s: 5A/div; i_d: 2A/div; v_{Cs}: 50V/div; v_{ds2}: 10V/div; time: 2μs/div)
(b)

Fig. 12. Conventional SP WPT waveforms. (a) Transmitter side and diode current. (b) Pickup.

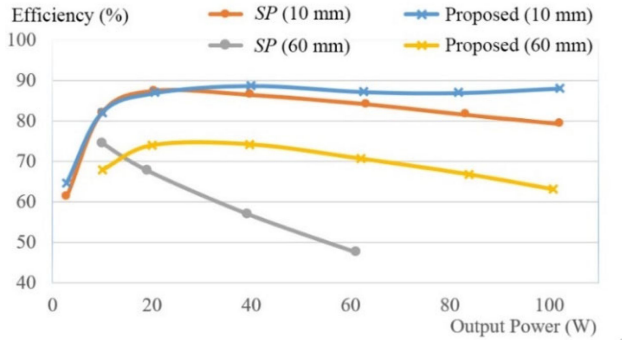

Fig. 13. Efficiency comparison curves.

input and output power are measured at the input dc port and output dc port, respectively. As load is heavier, only the center-tapped coil current difference becomes larger; therefore, conduction loss does not increase as the load. In addition, the transmitter-side current is also lower than that of the conventional SP compensated circuit, especially when the coupling is weak. Hence, the proposed circuit possesses much higher efficiency at heavy load and longer separation.

Fig. 14 shows the loss breakdown comparison on SP compensation and the proposed circuits. Both circuits deliver 60 W and both are with transmitter/pick-up windings 60-mm separation. The losses related with the transmitter winding current, e.g., MOSFET, Trans. Winding, Trans. Cap., and Input Cap., are more than doubled in the conventional SP compensation than in the

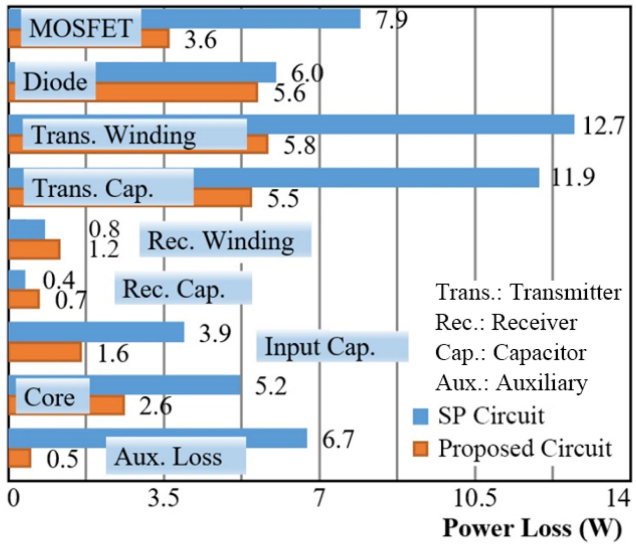

Fig. 14. Loss breakdown comparison.

proposed circuit. Contrarily, the losses related to the pickup winding currents are a little higher in the proposed circuit. The auxiliary loss accounts for the losses that cannot be attributed to. The reason why the proposed circuit outperforms conventional compensation can be explained by (4), (5), (12), and (13). Referring to Table I, the self-inductance L_{s1}/L_{s2} and mutual inductance M_{ss} do not differ too much. However, theoretically $M \approx 2M_{sp}$ and $L_s \approx 4L_{sc}$, since the two pickup windings in the proposed circuit have only half number of turns than in the SP circuit. From the equations, the pickup winding current of the proposed circuit is merely a little higher, whereas the transmitter winding current in the SP circuit is almost doubled compared to that in the proposed circuit. Similar comparison results can be applied to other compensation schemes such as *LCC* or *LCL* compensations, which are with nonsplit windings.

VI. Conclusion

This article proposes a WPT step-down converter with center-tapped pickup windings. Transmitter-side series compensation and pickup-side parallel compensation are adopted to increase the efficiency. A fundamental component analysis is applied to derive the winding currents as well as voltage gain of the proposed resonant circuit. By the proposed center-tapped pickup windings and compensation, the input impedance is proportional to the load impedance, and the voltage gain is less sensitive to the load variation. Since the load current is the difference between the two pickup windings, the efficiency is not satisfying at light load. Consequently, the proposed circuit is only comparable or even a bit worse than the conventional SP compensation topology at light load. However, it performs better at higher load conditions especially when the coupling is poor. The derived theoretical winding currents can help to comprehend this effect. According to the experiment, the best efficiency reaches 88.8% when coil separation is 10 mm and 74.3% when separation is 60 mm. The worst efficiency is 63.2% happening at 100-W load 60-mm separation.

REFERENCES

[1] R. Sedehi *et al.*, "A wireless power method for deeply implanted biomedical devices via capacitively coupled conductive power transfer," *IEEE Trans. Power Electron.*, vol. 36, no. 2, pp. 1870–1882, Feb. 2021.

[2] M. Schormans, V. Valente, and A. Demosthenous, "Practical inductive link design for biomedical wireless power transfer: A tutorial," *IEEE Trans. Biomed. Circuits Syst.*, vol. 12, no. 5, pp. 1112–1130, Oct. 2018.

[3] J. Pries, V. P. N. Galigekere, O. C. Onar, and G. J. Su, "A 50-kW three-phase wireless power transfer system using bipolar windings and series resonant networks for rotating magnetic fields," *IEEE Trans. Power Electron.*, vol. 35, no. 5, pp. 4500–4517, May 2020.

[4] J. Dai and D. C. Ludois, "A survey of wireless power transfer and a critical comparison of inductive and capacitive coupling for small gap applications," *IEEE Trans. Power Electron.*, vol. 30, no. 11, pp. 6017–6029, Nov. 2015.

[5] F. Lu, H. Zhang, H. Hofmann, and C. C. Mi, "An inductive and capacitive combined wireless power transfer system with LC-compensated topology," *IEEE Trans. Power Electron.*, vol. 31, no. 12, pp. 8471–8482, Dec. 2016.

[6] J. Shin *et al.*, "Design and implementation of shaped magnetic-resonance-based wireless power transfer system for roadway-powered moving electric vehicles," *IEEE Trans. Ind. Electron.*, vol. 61, no. 3, pp. 1179–1192, Mar. 2014.

[7] K. N. Mude and K. Aditya, "Comprehensive review and analysis of two-element resonant compensation topologies for wireless inductive power transfer systems," *Chin. J. Elect. Eng.*, vol. 5, no. 2, pp. 14–31, Jun. 2019.

[8] M. Ishihara, K. Umetani, and E. Hiraki, "Strategy of topology selection based on quasi-duality between series–series and series–parallel topologies of resonant inductive coupling wireless power transfer systems," *IEEE Trans. Power Electron.*, vol. 35, no. 7, pp. 6785–6798, Jul. 2020.

[9] Y. H. Liao and X. Q. Yuan, "Compensation topology for flat spiral coil inductive power transfer systems," *IET Power Electron.*, vol. 8, no. 10, pp. 1893–1901, Aug. 2015.

[10] S. Samanta and A. K. Rathore, "A new current-fed CLC transmitter and LC receiver topology for inductive wireless power transfer application: Analysis, design, and experimental results," *IEEE Trans. Transp. Electrific.*, vol. 1, no. 4, pp. 357–368, Dec. 2015.

[11] Y. H. Sohn, B. H. Choi, E. S. Lee, G. C. Lim, G. H. Cho, and C. T. Rim, "General unified analyses of two-capacitor inductive power transfer systems: Equivalence of current-source SS and SP compensations," *IEEE Trans. Power Electron.*, vol. 30, no. 11, pp. 6030–6045, Nov. 2015.

[12] R. Bosshard, J. W. Kolar, J. Mühlethaler, I. Stevanovi´c, B. Wunsch, and F. Canales, "Modeling and η-α-pareto optimization of inductive power transfer coils for electric vehicles," *IEEE J. Emerg. Sel. Top. Power Electron.*, vol. 3, no. 1, pp. 50–64, Mar. 2015.

[13] M. Lu and K. D. T. Ngo, "Systematic design of coils in series–series inductive power transfer for power transferability and efficiency," *IEEE Trans. Power Electron.*, vol. 33, no. 4, pp. 3333–3345, Jun. 2018.

[14] W. Zhang, S. C. Wong, C. K. Tse, and Q. Chen, "Load-independent duality of current and voltage outputs of a series- or parallel-compensated inductive power transfer converter with optimized efficiency," *IEEE J. Emerg. Sel. Top. Power Electron.*, vol. 3, no. 1, pp. 137–146, Mar. 2015.

[15] M. Budhia, J. T. Boys, G. A. Covic, and C. Y. Huang, "Development of a single-sided flux magnetic coupler for electric vehicle IPT charging systems," *IEEE Trans. Ind. Electron.*, vol. 60, no. 1, pp. 318–328, Jan. 2013.

[16] K. A. Kalwar, S. Mekhilef, M. Seyedmahmoudian, and B. Horan, "Coil design for high misalignment tolerant inductive power transfer system for EV charging," *Energies*, vol. 9, no. 11, pp. 937–949, 2016.

[17] S. Raabe and G. A. Covic, "Practical design considerations for contactless power transfer quadrature pick-ups," *IEEE Trans. Ind. Electron.*, vol. 60, no. 1, pp. 400–409, Jan. 2013.

[18] Z. Yi, M. Li, B. Muneer, and Q. Zhu, "High-efficiency mid-range inductive power transfer employing alternative-winding coils," *IEEE Trans. Power Electron.*, vol. 34, no. 7, pp. 6706–6721, Jul. 2019.

[19] H. Hao, G. A. Covic, and J. T. Boys, "An approximate dynamic model of LCL-T-based inductive power transfer power supplies," *IEEE Trans.Power Electron.*, vol. 29, no. 10, pp. 5554–5567, Oct. 2014.

[20] S. Li, W. Li, J. Deng, T. D. Nguyen, and C. C. Mi, "A double-sided LCC compensation network and its tuning method for wireless power transfer," *IEEE Trans. Veh. Technol.*, vol. 64, no. 6, pp. 2261–2273, Jun. 2015.

[21] C. S. Wong, Y. P. Chan, L. Cao, L. Wang, K. H. Loo, and M. C. Wong, "A single-stage dynamically compensated IPT converter with unity power factor and constant output voltage under varying coupling condition," *IEEE Trans.Power Electron.*, vol. 35, no. 10, pp. 10121–10136, Oct. 2020.

[22] H. Zhang, Y. Chen, C. H. Jo, S. J. Park, and D. H. Kim, "DC-link and switched capacitor control for varying coupling conditions in inductive power transfer system for unmanned aerial vehicles," *IEEE Trans. Power Electron.*, vol. 36, no. 5, pp. 5108–5120, May 2021.

[23] X. Qu, Y. Yao, D. Wang, S. C. Wong, and C. K. Tse, "A family of hybrid IPT topologies with near load-independent output and high tolerance to pad misalignment," *IEEE Trans. Power Electron.*, vol. 35, no. 7, pp. 6867–6877, Jul. 2020.